Review

NONLINEAR OPTICS IN WAVEGUIDE ARRAYS AND PHOTONIC NANOWIRES

TRAN XUAN TRUONG[†]

Department of Physics, Le Quy Don University, 236 Hoang Quoc Viet, Hanoi, Vietnam

[†]*E-mail:* tranxtr@gmail.com

Abstract. *In this paper we review our works in the field of nonlinear optics in waveguide arrays (WAs) and photonic nanowires. We first focus on the new equation governing light propagation in optical fibers with sub-wavelength cores which simultaneously takes into account (i) the vector nature of the electromagnetic modes inside fibers, (ii) the strong dispersion of the nonlinearity inside the spectral body of the pulse, (iii) and the full variations of the vector mode profiles with frequency. From this equation we have shown that a new kind of nonlinearity emerges in subwavelength-core fibers which can suppress the Raman self-frequency shift of solitons. We then discuss some nonlinear phenomena in WAs such as the emission of the diffractive resonant radiation from spatial discrete solitons and the anomalous recoil effect. Finally, we review our works on the optical analogues of Dirac solitons in quantum relativistic physics in binary waveguide arrays for both fundamental and higher-order solitons, and its interaction.*

Keywords: nonlinear optics, waveguide array, photonic nanowire, soliton, diffractive resonant radiation, Dirac soliton.

Classification numbers: 42.65.Tg, 42.81.Dp, 42.82.Et.

I. INTRODUCTION

Optical fibers [1, 2] and waveguide arrays (WAs) [3, 4] are optical systems exhibiting many important and interesting nonlinear phenomena, and are fundamental components of the modern optical technologies from both the fundamental and practical viewpoints. Evolution equations that accurately describe the propagation of short pulses in nonlinear media are extremely valuable tools in modern nonlinear optics, especially in fiber optics [1, 2]. Different approximations based on various versions of the nonlinear Schrödinger equation (NLSE) have been used quite successfully

in the past to describe a variety of linear and nonlinear effects in large-core optical fibers. Amongst them, we can mention phenomena such as soliton propagation [1,5], modulational instabilities and four-wave mixing [1], and third and higher-order dispersive effects [1]. An extended version of the NLSE (also called the generalized NLSE, or GNLSE), which also includes terms describing the Raman effect [6], self-steepening and the full complexity of the group velocity dispersion (GVD) of the optical fiber [1], has been used to describe the important phenomenon of supercontinuum generation (SCG) with striking success [7]. This equation has led to important advances in the theoretical understanding of SCG in ultra-small core fibers such as tapered fibers [8] and photonic crystal fibers (PCFs) [9, 10]. In particular, the phenomena of emission of solitonic dispersive resonant radiation [11] and the stabilization of the Raman self-frequency shift (RSFS) of solitons by means of such radiation [12, 13] are recent important advances that can be explained by the GNLSE.

The GNLSE is based on several approximations. The most important approximation used in all NLSEs is the slowly-varying envelope approximation (SVEA) in both space and time [1]. This approximation is only possible if the envelope profile contains many oscillations, which are typically the case in the visible and mid infrared regime when the pulse duration is larger than a few tens of femtoseconds. SVEA reduces the second-order wave equation for the electric field into a first-order equation in which the evolution coordinate is z, the longitudinal spatial coordinate along the fiber. Therefore, the computational complexity in simulations is hugely reduced.

The most crucial assumption on which the GNLSE is based is that the z-component of the electric field is very small with respect to its transverse components. The weak guidance regime represents a very good assumption for large-core fibers and for fibers with a low contrast between the refractive indices of the core and the cladding. Recently, however, new types of waveguides with a sub-wavelength size of the core (broadly referred to as photonic nanowires) have been successfully fabricated. The first class of these photonic nanowires is step-index silica wires with sub-wavelength cores [14]. The second class of these photonic nanowires possesses a complex cladding structure that allows one to support solid cores with a sub-wavelength diameter, and have a strong contrast between the refractive indices of the core and the cladding. To this class of waveguides belong some specific examples of PCFs, such as the extremely small interstitial features of Kagome hollow-core PCFs [15], and tapered fibers, i.e. silica rods with sub-micron diameters surrounded by air or vacuum [8]. As mentioned above, the common feature of all these structures is the non-negligible nature of the longitudinal component of the electric field (strong guidance regime) [16]. The importance of such component in the dynamics of light has not been clearly recognized in the past, until very recently [16]. In this latter work the authors demonstrate that the calculation of the nonlinear coefficient of photonic nanowires performed in the scalar theory [17–19] underestimates its real magnitude of approximately a factor 2, while the correct result can be found by using the more complete vector theory [16].

Inspired by these recent achievements, in our works [20, 21] we have advanced further the theoretical understanding of the evolution equations in optical fibers with sub-wavelength core structures. In [20, 21] we have derived a new, logically self-consistent forward-evolution equation for photonic nanowires, based on SVEA, that simultaneously takes into account (i) the vector nature of the EM field (polarization and z-component included), (ii) the strong dispersion of the nonlinearity inside the spectral body of the pulse, and (iii) the full variations of the vector mode

profiles with frequency. In all relevant previous works on the subject [16, 22–25], all these properties were not included in the derivation at the same time. Considering (i), (ii) and (iii) altogether and with a minimal amount of assumptions, leads to new qualitative results that have not been possible to investigate with previous formulations. In particular, we have demonstrated analytically and through a series of accurate simulations that (iii) leads to the emergence of new nonlinear terms that are also indirectly responsible for appreciable modifications in the dynamics of RSFS, in particular a suppression of the latter. Thus, even though the vector nature of the electromagnetic (EM) field in photonic nanowires may lead to an enhancement of the nonlinear coefficient [16], our results show that this is actually counterbalanced by terms and effects that partially suppress such enhancement. These recent results of our works will be reviewed later in Sec. II.

Waveguide arrays consisting of identical, equally spaced waveguides, present a unique discrete platform to explore many interesting fundamental phenomena such as discrete diffraction [4, 26], discrete solitons [27, 28]. Recently, WAs have been used intensively to simulate the evolution of non-relativistic quantum mechanical particles in a periodic potential. Many fundamental phenomena in nonrelativistic classical and quantum mechanics, such as Bloch oscillations [29, 30], Zener tunneling [31, 32], optical dynamical localization [33], and Anderson localization in disordered lattices [34] have been simulated both theoretically and experimentally with WAs. Recently, binary waveguide arrays (BWAs) have also been used to mimic relativistic phenomena typical of quantum field theory, such as Klein tunneling [35, 36], the Zitterbewegung (trembling motion of a free Dirac electron) [37, 38], and fermion pair production [39], which are all based on the properties of the Dirac equation [40]. Although there is as yet no evidence for fundamental quantum nonlinearities, nonlinear versions of the Dirac equation have been studied for a long time. One of the earlier extensions was provided by Heisenberg [41] in the context of field theory and was motivated by the question of mass. In the quantum mechanical context, nonlinear Dirac equations have been used as effective theories in atomic, nuclear and gravitational physics [42–45]. In this regard, BWAs can offer a quite unique model system to simulate nonlinear extensions of the Dirac equation when probed at high light intensities.

In this work we review our recent results on nonlinear phenomena in WAs and BWAs. First, we review our discovery of the diffractive resonant radiation [46 – 48] in WAs in Sec. III. Then, in Sec. IV we move on to review ours latest works on the optical analogues of the quantum relativistic Dirac solitons in BWAs [49–52]. Finally, the conclusions are given in Sec. V.

II. NEW NONLINEARITY IN PHOTONIC NANOWIRES

In this Section we review our works on the new equation governing light propagation in optical fibers with sub-wavelength core [20] and the new kind of nonlinearity emerging in these fibers [21].

II.1. Light propagation equation in fibers with sub-wavelength core

As mentioned in the Introduction, in conventional optical fibers the core is much larger than the wavelength, thus the EM modes of these fibers can be considered transverse. In this case, it is quite safe to ignore the *z*-component of the EM mode, the dispersion of the nonlinearity coefficient, and the variation of mode profiles with respect to wavelength. In this circumstance, the GNLSE can be used successfully and has become standard in large-core optical fibers [1]. However, for optical fibers with sub-wavelength cores all these assumptions, and thus GNLSE, become
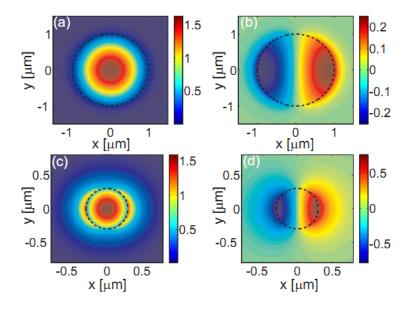
Fig. 1. (a,b) Transverse and longitudinal components of the electric field, respectively, in a silica strand in air of diameter $d = 2\ \mu m$, for a pump wavelength $\lambda = 1\ \mu$m. (c,d) The same as (a,b), but for diameter $d = 0.6\ \mu$m. The silica core is indicated with a dashed black line. Note the expulsion of the total field from the core towards the low-index medium and the enhancement of the z-component for small cores. This figure is reproduced from our original work in Ref. [20].

problematic. For instance, the z-component of the EM mode now is more enhanced and one cannot neglect it. As an example, in Fig. 1 we show the transverse and longitudinal components of EM modes in a silica strand in air [20]. As shown in Fig. 1(a,b), when the diameter of the core ($d = 2\ \mu$m) is larger than the wavelength ($\lambda = 1\ \mu$m) one can see that the transverse component (Fig. 1(a)) is much stronger than the z-component. However, when the core size is reduced to $d = 0.6\ \mu$m as in Fig. 1(c,d) the z-component becomes pronounced. This enhancement of the z-component is even stronger for smaller cores. In order to take into account the above-mentioned distinguishing features of fibers with sub-wavelength core, in our works [20, 21] we describe the variations of the normalized EM mode $\hat{\vec{e}}_{\omega}(\vec{r}_{\perp})$ (where $\vec{r}_{\perp}$ are the transverse coordinates) with respect to the frequency ω through the Taylor series:

$$\hat{\vec{e}}_{\omega}(\vec{r}_{\perp}) = \sum_{j \geq 0} \frac{1}{j!} \vec{f}^{(j)}_{\omega_0}(\vec{r}_{\perp}) \left(\frac{\Delta\omega}{\omega_0} \right)^{j}, \tag{1}$$

where $\Delta\omega = \omega - \omega_0$ is the frequency detuning from an arbitrary reference frequency ω_0 and the quantity $\vec{f}^{(j)}_{\omega_0}$ is proportional to the jth frequency derivative of the mode profile. As shown in detail in Ref. [20] one can rigorously prove that the equation governing the light propagation of the fundamental EM mode of the photonic nanowires is given by:

$$i\partial_z Q + \hat{D}(i\partial_t)Q + \sum_{jhpv} \gamma^{jhpv} \hat{G}^j(i\partial_t)\varphi^{hpv} = 0. \tag{2}$$

In Eq. (2) letters j, h, p, v are used for derivative indices, $Q(z,t)$ is the electric envelope, $\hat{D}(i\partial_t) \equiv \beta(\omega_0 + i\partial_t) - \beta(\omega_0)$ is the conventional dispersion operator that contains all information on the fiber GVD around ω_0 [1], β is the ω-dependent propagation constant of the fundamental mode, $\hat{G}^j(i\partial_t) \equiv [1 + (i/\omega_0)\partial_t][(i/\omega_0)\partial_t]^j$ is the operator which contains the shock term [1] and the zeroth order of the Taylor expansion ($j = 0$). The convoluted nonlinear fields in Eq. (2) are defined as follows (see Ref. [20] for more details):

$$\varphi^{hpv}(z,t) \equiv \frac{[(i\partial_t)^h Q]\{R \otimes ([(i\partial_t)^p Q][(-i\partial_t)^v Q*])\}}{\omega_0^{h+p+v}}, \qquad (3)$$

where symbol $\otimes$ denotes a time convolution. In Eq. (3) $R(t) \equiv (1\text{-}\theta)\delta(t) + \theta h(t)$ is the nonlinear response function of the core which includes the instantaneous Kerr (1st term) and the non-instantaneous Raman (2nd term) with θ being the relative importance between the two [1]. Note that in Eq. (3), $\varphi^{000} = Q \int R(t-t')|Q(t')|^2 dt'$ gives the conventional, zeroth order convolution that is used in GNLSE [1]. The generalized nonlinear coefficient γ^{jhpv} is defined as follows (see Refs. [20, 21] for more details):

$$\gamma^{jhpv}(\omega_0) \equiv \frac{\omega_0}{16c} \int d\vec{r}_\perp \chi^{(3)}_{xxxx}(\vec{r}_\perp) \frac{\left(\begin{array}{c}\left[\vec{f}^{*(j)}_{\omega_0} \cdot \vec{f}^{(h)}_{\omega_0}\right]\left[\vec{f}^{(p)}_{\omega_0} \cdot \vec{f}^{*(v)}_{\omega_0}\right] + \left[\vec{f}^{*(j)}_{\omega_0} \cdot \vec{f}^{(p)}_{\omega_0}\right]\left[\vec{f}^{(h)}_{\omega_0} \cdot \vec{f}^{*(v)}_{\omega_0}\right] \\ + \left[\vec{f}^{*(j)}_{\omega_0} \cdot \vec{f}^{*(v)}_{\omega_0}\right]\left[\vec{f}^{(h)}_{\omega_0} \cdot \vec{f}^{(p)}_{\omega_0}\right]\end{array}\right)}{j!h!p!v!}, \quad (4)$$

where $\chi^{(3)}_{xxxx}$ is the third-order susceptibility which is a function of the transverse coordinates in the waveguide. Eq. (4) is a generalization of the nonlinear coefficient commonly used in fiber optics [1], and takes into account the full vector nature of the field profile as well as its frequency variation. Such variations are at the very core of the new nonlinearities described in the next subsection, since the Taylor series of Eq. (1) implies the existence of an infinite number of additional terms that depend on higher-order time derivatives of the envelope. The quantities γ^{jhpv} satisfy some symmetry relations [20] that significantly reduce the number of independent nonlinear coefficients for each order of the derivative: $\gamma^{jhpv} = \gamma^{vhpj} = \gamma^{jphv} = \gamma^{vphj}$, $\gamma^{jhhh} = \gamma^{hjhh}$, $\gamma^{jhhj} = \gamma^{hjjh}$.

II.2. A new kind of nonlinearity in photonic nanowires

As mentioned above, higher-order derivatives of the mode profiles embedded into Eq. (3) are responsible for the emergence of new nonlinear terms. These new terms obviously become increasingly small with increasing order of derivatives, since for every derivation there is a factor $1/\omega_0$. However, as demonstrated in Refs. [20, 21], the new first order term has a strength comparable with or sometimes even larger than the Raman term. In this subsection, we just focus on the two dominant nonlinear coefficients: the conventional zeroth-order and the new first-order coefficients. From the expression in Eq. (4) one can define the zeroth-order nonlinear coefficient of the optical fiber [21]: $\gamma_0 = \gamma^{0000}$, which is a conventional definition of the nonlinear coefficient in fiber optics [1]. To the first-order expansion in Eq. (2) one can define the coefficient $\gamma_1 = \gamma^{1000}/(\omega_0 t_0)$, associated with nonlinear convoluted fields that contain only one time derivative of the envelope. Then, in Ref. [20] we have shown that one can obtain the following evolution equation for long

pulses:

$$i\partial_z Q + \hat{D}(i\partial_t)Q + \gamma_0 \left[\underbrace{\left(1 + \frac{i}{\omega_0}\partial_t\right)}_{T0} \underbrace{|Q|^2 Q}_{T1} - \underbrace{T_R Q \partial_t |Q|^2}_{T2} \right] + \underbrace{\frac{4i\gamma_1}{\omega_0}|Q|^2 \partial_t Q}_{T3} = 0. \qquad (5)$$

In Eq. (5), the term indicated by $T0$ represents the well-known shock operator [1]. Terms $T1$ and $T2$ in Eq. (5) correspond to the conventional Kerr effect and Raman self-frequency shift, respectively, where $T_R = \int_{-\infty}^{\infty} t' R(t') dt'$ is the first moment of the Raman nonlinear response function [1]. The additional term $T3$ is connected to a nonlinear change of the group velocity. This nonlinear term is strictly related to the mode profile variations with respect to the frequency.
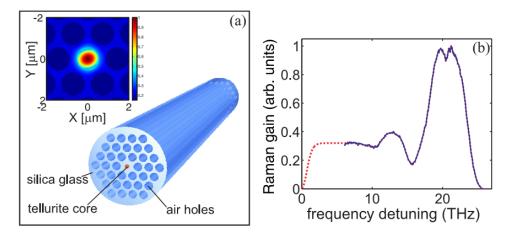

Fig. 2. (a) Schematics of the proposed PCF nanowire geometry. The central nanowire core is made of tellurite glass ($77TeO_2$ -$10Na_2O$ - $10ZnO$- $3PbO$ composition from Ref. [53]), while the cladding is made of silica with a triangular lattice of air holes. Parameters of the PCF are pitch Λ = 1.4 μm, air hole radius R = 0.56 μm, core radius R_c = 0.5 μm. Inset: The density plot of the mode profile intensity of the waveguide for λ = 1.55 μm is shown. (b) Profile of the Raman gain spectrum for the tellurite glass. Solid blue line, experimental data taken from Ref. [53]; dotted red line, fit used in our simulations. This figure is reproduced from our original work in Ref. [21].

In Ref. [20] we considered only the circular geometry for photonic nanowires. However, circular strands of high-refractive index material in a homogeneous cladding, including in air, are not optimal for experimentally detecting the effects of new nonlinear terms, because the maximum of the new nonlinear coefficient is located, as a rule, far away in a region of strong normal dispersion, where bright solitons cannot exist. In fact, as has been anticipated in Ref. [20], the new nonlinearity is visible only in the presence of solitons, and its effects are nearly invisible in the normal dispersion regime. In Ref. [21] we have proposed to use a silica-based PCF with a triangular arrangement of the air holes (see Fig. 2(a)). In Ref. [21] we have demonstrated that, by means of careful choice of parameters in the design of PCFs, one can move the maximum of the new nonlinearity inside the region of anomalous dispersion. This will make it much easier

to observe the new nonlinearity experimentally, and can cause a considerable suppression of the RSFS of the soliton from the very start of the propagation.
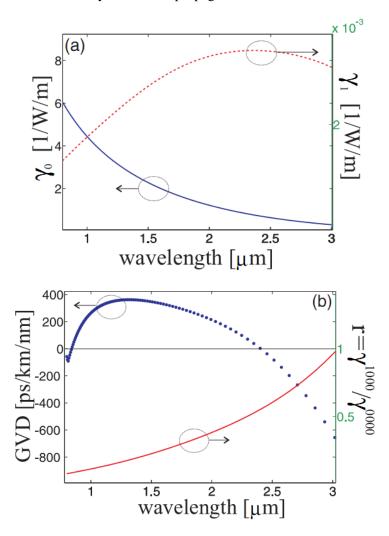

Fig. 3. Linear and nonlinear data for the PCF design of Fig. 2(a). (a) Blue solid and red dashed lines indicate, respectively, γ_0 and γ_1 versus wavelength. (b) Blue dots indicate the GVD of the waveguide, with zero-GVD points located at $\lambda = 0.84$ μm and $\lambda = 2.4$ μm. Red solid line indicates parameter $r = \gamma^{1000}/\gamma^{0000}$. This figure is reproduced from our original work in Ref. [21].

Figure 3(a) shows plots of γ_0 and γ_1 versus reference wavelength for the fiber design in Fig. 2(a). The fiber GVD is shown in Fig. 3(b) with blue dots. It is clear from this figure that γ_0 decreases monotonically for longer wavelengths (a well-known fact). However, it is interesting to note that the new nonlinear coefficient γ_1 initially increases, but then reaches a maximum near the infrared zero-GVD point of the fiber (located at $\lambda = 2.4$ μm), and then tends to zero for even longer wavelengths. The close vicinity of max(γ_1) to the anomalous GVD of the fiber is an

atypical feature that we have found only in a few very specific designs, including the one presented in Fig. 2(a). The "normal" situation, which is also true for circular photonic nanowires surrounded by homogeneous media (such as, for instance, tapered fibers), is that $\max(\gamma_1)$ is located well within the region of normal GVD [20].

We now show that the emergence of the new nonlinearity leads to a strong suppression of the RSFS. In order to do this, we compare two direct numerical simulations of pulse propagation, the first one obtained by truncating the expansion of Eq. (2) to the zeroth order (one nonlinear convolution, corresponding to the conventional GNLSE) (Fig. 4(a)), the second one obtained by truncating the same sum to the second-order (15 nonlinear convolutions in total), which thus takes into account the dominant terms of the new nonlinearities (Fig. 4(b)). It is easily seen by comparing Fig. 4(a) with Fig. 4(b) that the net effect of the additional nonlinearities is to reduce considerably the RSFS in the fiber. Thus a unique interplay between the new nonlinearities and the RSFS takes place in properly designed photonic nanowires. It is possible to qualitatively understand the reason of the above RSFS suppression mechanism by using the so-called moment method which keeps tracks of the solitonic parameters under the influence of small perturbations (see Ref. [21] for more details).
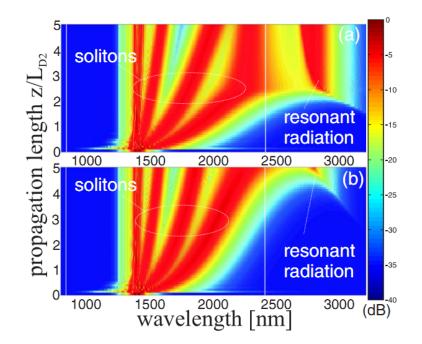

Fig. 4. (a) Density plot showing nonlinear evolution of a pulse with $t_0 = 150$ fs, $P = 1$kW in the waveguide of Fig. 2(a) according to Eq. (2) truncated at the 0th order, i.e., by using the conventional GNLSE. Second-order dispersion length is $L_{D2} = 6$ cm. (b) Same as (a) but truncating Eq. (2) at the 2nd order. Vertical white lines indicate the two zero-GVD wavelengths. This figure is reproduced from our original work in Ref. [21].

III. DIFFRACTIVE RESONANT RADIATION IN WAVEGUIDE ARRAYS

In this Section we review our works on discovery of the diffractive resonant radiation (DifRR) emitted by discrete spatial solitons in WAs. The concept of dispersive resonant radiation (DisRR), which is emitted from an optical pulse propagating in a single optical fiber due to higher-order dispersion terms, has been well studied in the temporal case [11]. When an ultra-short pulse is launched into an optical fibers, it can generate one or more new frequencies if the phase matching condition is satisfied [11]. This DisRR, together with other nonlinear effects such as self- and cross-phase modulation, soliton fission [54], and stimulated Raman scattering [55], are the main ingredients of the supercontinuum generation [1, 2, 56], particularly in highly nonlinear PCFs [9]. Supercontinuum generation is one of most important phenomena in nonlinear fiber optics which has led to a number of important technological advances in various fields, such as spectroscopy and medical imaging, metrology, and the realization of broadband sources [1].

Inspired by advances in DisRR studies, in one of our works [46] the DifRR which occurs when a continuous-wave (CW) beam or a relatively long pulse is launched into WAs has been discovered for the first time. Similarities and differences between DisRRs and DifRRs have been analyzed in Ref. [46]. We have shown that when the phase matching condition is satisfied, a spatial soliton emits DifRR with a new well-defined direction, i.e., a transverse wave number. Moreover, due to the periodicity of discrete systems, and thus the existence of a Brillouin zone, unusual effects which cannot exist in continuous media can now occur. One of these is the anomalous solitonic recoil described in Ref. [46] for the first time.

III.1. Phase matching condition for the diffractive resonant radiation

Light propagation in a discrete, periodic array of Kerr nonlinear waveguides can be described, in the CW regime, by the following well-known dimensionless coupled-mode equations (CMEs) [2, 4, 28]:

$$i\frac{da_n(z)}{dz} + c\left[a_{n+1}(z) + a_{n-1}(z)\right] + |a_n(z)|^2 a_n(z) = 0, \tag{6}$$

where a_n is the electric field amplitude in the nth waveguide, z is the longitudinal spatial coordinate, c is the coupling coefficient resulting from the field overlap between neighboring waveguides. By using the stationary discrete plane wave solution for the nth waveguide $a_n(z) = a_0 \exp[i(nk_x d + \kappa_z z)]$ one arrives, in the linear case, at the well-known dispersion relation between κ_z and k_x[4]:

$$\kappa_z(k_x) = 2c\cos(k_x d), \tag{7}$$

where d is the center-to-center spacing between two adjacent waveguides, and k_x is the transverse wave number; see the solid blue line of Fig. 5(a) . It is clear from Eq. (7) that κ_z is periodic in $\kappa \equiv k_x d$, which represents the phase difference between adjacent waveguides. Thus, within the coupled mode approximation, it suffices to investigate the first Brillouin zone of the folded dispersion, $-\pi \le \kappa \le \pi$.

Since a typical input beam has a finite width covering several waveguides, its Fourier spectrum has a certain bandwidth with a central transverse wave number κ_0, which is fixed by the input angle of incidence of the exciting beam. We can then use a Taylor expansion of Eq. (7) as follows:

$$\kappa_z(\kappa) = \kappa_z(\kappa_0) + \sum_{m\ge 1}\frac{D_m}{m!}\Delta\kappa^m, \tag{8}$$

where $\Delta\kappa = \kappa - \kappa_0$, and $D_m = (d^m \kappa_z / d\kappa^m)|_{\kappa 0}$ is the mth order diffractive Taylor coefficient. In Fig. 5(a) we plot a typical curve for $D_2(\kappa)$ (dashed red line), showing the existence of two zero-diffraction points located at $\kappa = \pm\pi/2$. This shape of D_2 is analogous to the GVD of PCFs in the temporal case [9]. In Ref. [46], we made full use of this analogy when we describe the dynamics and the formation of the DifRR.

Following Ref. [4], we now approximate the discrete variable n with a continuous one. This is justified since we shall use pulses and solitons that extend for several waveguides (typically, 5 waveguides or more are enough for the continuous model to give excellent results), and this approximation is fully vindicated by our numerical simulations in the next subsection. Defining n as a continuous variable of the distributed amplitude function $a(n,z) \to a_{n,z} \exp(-i\kappa_0 n)$ we eliminate the zeroth order term $\kappa_z(\kappa_0)$, which is responsible for the general phase evolution through the substitution $a(n,z) \to a(n,z)\exp[i\kappa_z(\kappa_0)z]$. The first order term, $-iD_1 \partial_n$, takes into account the transverse velocity and can also be eliminated by introducing a comoving frame, $n \to n + D_1 z$. After dropping these two low-order terms one arrives at the following equation:

$$\left[i\partial_z - \frac{D_2}{2}\partial_n^2 + \sum_{m \geq 3} \frac{D_m}{m!}(-i\partial_n)^m + |a(n,z)|^2 \right] a(n,z) = 0. \tag{9}$$

Equation (9) is formally identical to the well-known GNLSE, which describes the evolution of pulses in a single optical fiber, plus higher-order dispersion (HOD) terms [1]. In Eq. (9) we have the transverse spatial variable n instead of the temporal variable t of the conventional GNLSE. Unlike the temporal GNLSE, where a Taylor series for the fiber dispersion can usually be expanded up to a small number of terms (because HOD coefficients become rapidly very small), in Eqs. (8) and (9) many higher-order diffraction terms $D_{m \geq 2}$ should be taken into account, since their absolute values will be either $|2c \sin(\kappa_0)|$ or $|2c \cos(\kappa_0)|$, and the sum only converges due to the factorial in the denominator.

In the temporal version of the GNLSE, it is well known that a temporal soliton propagating in a fiber emits small amplitude, dispersive, and quasimonochromatic waves at well-defined frequencies (the DisRR) when the linear fiber dispersion and the nonlinear soliton dispersion (which is constant and proportional to its peak power) are matched [11, 13]. It is thus natural to conjecture that, in a WA, a spatial soliton, which in the continuous variable approximation extends over several waveguides, emits during the propagation a similar kind of small-amplitude diffractive radiation, within a narrow wave number range, due to the phase matching between the spatial soliton nonlinear dispersion and the linear array dispersion given by Eq. (7). By using the perturbation approach, which was developed for DisRRs [11], in Ref. [46] we have derived the phase-matching condition for the DifRR in a similar way. We first nd the unperturbed soliton solution of Eq. (9) where all diffractive terms $D_{m \geq 3}$ are dropped. Under these conditions, the soliton solution is given by:

$$a_{\rm sol}(z,n) = A_0 {\rm sech}\left(\frac{nA_0}{\sqrt{2c\cos(\kappa_0)}} \right) \exp(ik_{\rm sol}z), \tag{10}$$

where $k_{sol} = A_0^2/2$ is the spatial soliton longitudinal wave number, identical to its temporal counterpart. The bright soliton solution (10) only exists when $2c \cos(\kappa_0) ¿ 0$, i.e., only in half of the Brillouin zone, where $-\pi/2 \leq \kappa_0 \leq \pi/2$. Now we look for the linearized dispersion relation of plane wave solutions of Eq. (9), by substituting $\exp[i(k_{lin}z + \Delta\kappa n)]$ into Eq. (9) and using Eq. (8).
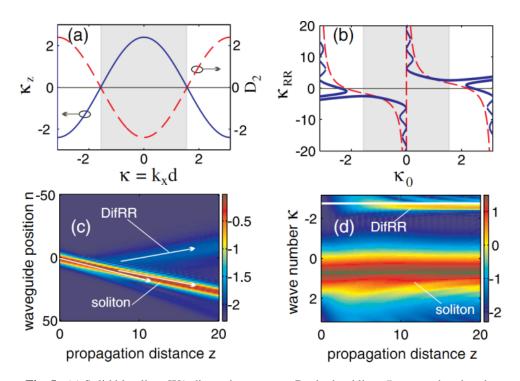
Fig. 5. (a) Solid blue line: WA dispersion κ_z vs κ. Dashed red line: D_2 vs κ, showing the two zero-diffraction points located at $\kappa = \pm\pi/2$. (b) Wave number κ_{RR} of the generated DifRR, as a function of the input soliton wave number κ_0. The red dashed line indicates the approximated formula $\kappa_{RR} \approx \kappa_0 + 3/\tan(\kappa_0)$ for the position of the resonant radiation, while the blue solid line is the result of the exact implicit formula given by Eqs. (11) and (12). In both (a) and (b) the gray shaded area indicates the region where bright solitons can propagate. (c),(d) Beam propagation in the (n, z) plane (c) and (κ, z) plane (d). Parameters are $A_0 = 0.8$, $c = 1.2$, $\kappa_0 = 0.7$. This figure is reproduced from our original work in Ref. [46].

We obtain:

$$k_{\lin}(\Delta\kappa) \equiv \sum_{m \geq 2} \frac{D_m}{m!} \Delta\kappa^m = 2c\left[\cos(\kappa) - \cos(\kappa_0) + \sin(\kappa_0)\Delta\kappa\right]. \tag{11}$$

In Eq. (11), κ_0 is the central wave number (which is related to the incident angle) of the incident beam, while $\Delta\kappa$ is the detuning from κ_0, and $\kappa = \kappa_0 + \Delta\kappa$. Energy exchange between radiation and solitons is possible for those values of $\Delta\kappa$ that satisfy

$$k_{\lin}(\Delta\kappa) = k_{\sol}, \tag{12}$$

where k_{sol} is constant and has been defined above. This phase matching condition, an implicit equation for the radiation wave number detuning $\Delta\kappa$, is the central result of our work in Ref. [46]. It is important to note that although the phase-matching condition expressed in Eq. (12) has been derived from the continuous model of Eq. (9), such a formula very accurately predicts the DifRR wave number in the full original discrete model of Eq. (6), as we shall show below.

Incidentally, if we would have followed what is commonly done for optical fibers, i.e., taking into account only D_2 and D_3 in Eq. (11), and ignoring the power dependence ($k_{sol} \to 0$), one can easily get the approximate DifRR wave number in the form $\kappa_{RR} \approx \kappa'_{RR} = \kappa_0 + 3/\tan(\kappa_0)$. Such approximations are perfectly fine in fiber optics when dealing with DisRR — they lead to very accurate predictions of the DisRR frequency. However, the same approximation is not good enough for the case of WAs, since, as explained above, the coefficients ($D_m/m!$) decay not as rapidly as in the temporal case, and a large number of orders must be taken into account, as we show explicitly in the next section. However, even if not explicit as in the case of the temporal DisRR, Eq. (12) is exact and can be easily solved numerically.

III.2. Emission of DifRR and soliton anomalous recoil

We now prove numerically the formation of DifRR in the full discrete model of Eq. (6), and the accuracy of the predictions made by the phase-matching condition Eq. (12).

In Fig. 5(b) we show the DifRR wave number $\kappa_{RR} = \kappa_0 + \Delta\kappa$ as a function of the input soliton wave number (which is related to the angle of incidence) κ_0. The blue solid curve is obtained by finding numerically the roots $\Delta\kappa$ of Eq. (12), while the dashed red curve shows the approximated analytical expression given in the previous section. It is clear that k'_{RR} is not accurate enough to be used in practice, when compared to the solid line, which shows a complexity that goes beyond any truncation of the Taylor expansion in Eq. (3), especially when the power dependence is included via the right-hand side of Eq. (7).

In Fig. 5(b) we depict the full range of the first Brillouin zone for completeness, but only the interval $-\pi/2 \le \kappa_0 \le \pi/2$ (indicated by a gray shaded area), in which pulses experience "anomalous" diffraction (i.e., $D_2 < 0$), should be considered, since this is the only region where solitons can form in the WA (for focusing nonlinearity), analogously to the anomalous dispersion frequency range of optical fibers. Parameters used in Fig. 1 are $A_0 = 0.8$, $c = 1.2$, and $\kappa_0 = 0.7$. For these parameters, in the range $0.235 < |\kappa_0| < \pi/2$, one can find only one solution for κ_{RR}, but when $0 < |\kappa_0| < 0.235$, Eq. (12) shows several roots (see the solid blue curve in Fig. 5(b)). Thus, one should expect to simultaneously generate several DifRRs with different wave numbers in the latter interval. However, full numerical simulations of Eq. (6) show that only the solution corresponding to the branch that is the closest to the central horizontal axis (i.e., the axis $\kappa_{RR} = 0$) can be generated and observed, and all other DifRR waves corresponding to roots from other branches are too weak to be seen numerically, since the overlap between the soliton spectral tail and the radiation wave numbers becomes exponentially small. When $\kappa_0 = 0$, i.e., for a normal incidence of the input CW beam, there is no solution for Eq. (12), regardless of the parameters used. This is also confirmed by the direct simulation of Eq. (6).

The evolution of a CW beam along z according to Eq. (6) is shown in Fig. 5(c). After some propagation, around $z = 3$, a DifRR is emitted by the soliton. The evolution of the Fourier transform of the field $a(n)$ of Fig. 5(c) along z is shown in Fig. 5(d). The dashed green horizontal line represents the input wave number ($\kappa_0 = 0.7$), while the solid white line is obtained by solving Eq. (12) numerically, showing excellent agreement with the pulse propagation. In Fig. 5(b) one can notice that the soliton emits the DifRR with a positive detuning $\Delta\kappa$ when $0 < \kappa_0 < \pi/2$. For instance, when $\kappa_0 = 0.7$, then from Eq. (12) one gets $\kappa_{RR} = \kappa_0 + \Delta\kappa = 3.53$. However, since the Brillouin zone has a limited extension, when $2\pi > \kappa_{RR} > \pi$ the DifRR will be emitted with a negative detuning due to the folding of the band structure. In the example shown in Fig. 5(d)

the effective DifRR wave number will be equal to $\kappa_{RR} - 2\pi \approx -2.75$ (see the white solid line in Fig. 5(d)). This means that in real space the soliton, instead of recoiling in an opposite direction than the DifRR, will recoil towards the DifRR itself, see the white arrows in Fig. 5(c). The same phenomenon occurs in the wave number space: the soliton spectral momentum, instead of recoiling away from the radiation, moves slightly towards it (see Fig. 5(d)). We call this unique effect (which cannot be found in continuous media such as fibers due to the lack of a Brillouin zone) anomalous recoil. This kind of anomalous recoil in WAs takes places not only with the DifRR, but also with other beams and discrete solitons as investigated in details in our recent work [48] where we analyze the control of a strong discrete soliton by a much weaker beam. In Ref. [47] we have shown that the emission of DifRRs is a universal effect in WAs and it takes place not only with optical beams, but also with pulses launched into the system.

IV. DIRAC SOLITONS IN BINARY WAVEGUIDE ARRAYS

Waveguide arrays investigated in Section III consist of identical waveguides which are periodically laid next to each other in such a way that their individual modes overlap. As mentioned in the Introduction, WAs have been used intensively to simulate many fundamental phenomena in nonrelativistic classical and quantum mechanics. However, it was a common belief that the use of WAs as a model system for quantum mechanics carries the intrinsic drawback of being limited to nonrelativistic phenomena. Only recently, it turns out that binary waveguide arrays - an alternating sequence of two different types of waveguides - can be used to mimic relativistic phenomena typical of quantum field theory, such as Klein tunneling [35, 36], the Zitterbewegung [37, 38], and fermion pair production [39], which are all based on the properties of the Dirac equation [40]. In this Section we review ours latest works on the optical analogues of the quantum relativistic Dirac solitons in BWAs [49–52].

IV.1. Analytical soliton solutions in binary waveguide arrays

Light propagation in a discrete, periodic BWA of Kerr nonlinearity can be described, in the CW regime, by the following dimensionless coupled-mode equations [57]:

$$i\frac{da_n(z)}{dz} = -c\left[a_{n+1}(z) + a_{n-1}(z)\right] + (-1)^n \sigma a_n - \gamma |a_n(z)|^2 a_n(z), \tag{13}$$

where 2σ is the propagation mismatch between two adjacent waveguides of the array, and γ is the nonlinear coefficient of waveguides, which is positive for self-focusing, but negative for self-defocusing media. In the dimensionless form, in general, one can normalize variables in the above equation such that both γ and c are equal to unity in the self-focusing case. However, throughout our works in [49, 52] and in this Section these parameters are kept explicitly in Eq. (13). The only difference between Eq. (6) and Eq. (13) is that in Eq. (13) there is a new term containing σ which emerges due to the binary character of the new system. In [49] we have found the analytical solutions for fundamental Dirac solitons as follows:

$$\begin{bmatrix} a_{2n}(z) \\ a_{2n-1}(z) \end{bmatrix} = \begin{bmatrix} i^{2n}\frac{2c}{n_0\sqrt{\sigma\gamma}}\text{sech}\left(\frac{2n}{n_0}\right)e^{iz\left(\frac{2c^2}{n_0^2\sigma}-\sigma\right)} \\ i^{2n}\frac{2c^2}{n_0^2\sigma\sqrt{\sigma\gamma}}\text{sech}\left(\frac{2n-1}{n_0}\right)\tanh\left(\frac{2n-1}{n_0}\right)e^{iz\left(\frac{2c^2}{n_0^2\sigma}-\sigma\right)} \end{bmatrix}. \tag{14}$$

This analytical Dirac soliton solution in BWAs is a one-parameter family where one parameter, such as soliton peak amplitude or width, can be arbitrary, provided that the soliton width is large enough (the beam width parameter $n_0 \geq 3.5$, see Ref. [49] for more details). The Dirac soliton solution in the form of Eq. (14) is valid in the case when γ and σ are positive. However, with this solution one can easily construct other Dirac soliton solutions for any sign of each parameter γ and σ [49].
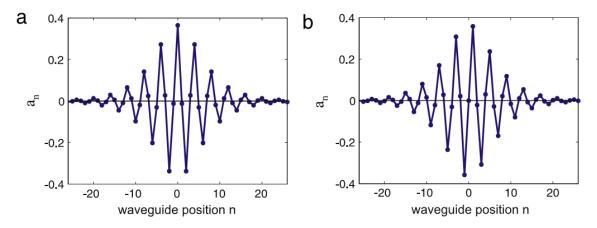

Fig. 6. Discrete soliton profiles (a, b) for even and odd symmetry, respectively. Full circles mark the field amplitudes across the BWA. Parameters in (a): $c = 1$; $\gamma = 1$; $\sigma = -1.2$; and $n_0 = 5$. This figure is reproduced from our original work in Ref. [49].

In Fig. 6(a) we plot the soliton profile with even symmetry calculated by using Eq. (14) at $z = 0$ with full circles marking the field amplitudes across BWAs, for the parameters given in the caption. Note that the soliton profile in Fig.6 (a) consists of two components: one strong component a_{2n} and another much weaker component a_{2n-1}(see also Fig. 7(c)). Once we get the soliton solution in Fig. 6(a), we can construct another soliton solution of the same physical system by changing the sign of σ and following the rules explained [49].

As an example, in Fig. 7(a) we show the soliton propagation along z as obtained by numerically solving Eq. (13) with an input soliton taken from Eq. (14) at $z = 0$, demonstrating that the soliton profile is well preserved during propagation. The parameters used for Fig. 7 are the same as in Fig. 6(a). The evolution of the Fourier transform of the field a_n in Fig. 7(a) along z is shown in Fig. 7(b), where the wave number k represents the phase difference between adjacent waveguides. Due to the periodic nature of BWAs, within the coupled mode approximation, it suffices to investigate κ in the first Brillouin zone $-\pi \leq \kappa \leq \pi$ [4]. One very important feature of the wavenumber evolution in Fig. 7(b) is the fact that there are two components of wavenumber centered at $\kappa = \pm\pi/2$ which correspond to two Bragg angles [38] with opposite inclinations. These two wavenumber components are generated at the input and preserve their shapes during propagation along z. This feature of k indicates that the soliton operates in the region where CMEs could potentially be converted into the relativistic Dirac equations describing the evolution of a freely moving relativistic particle [37, 38]. We will come back to this important point again later. Fig. 7(c) shows the two components of the soliton profile at odd and even waveguide positions n. The strong component with solid curves and square markers represents the field profile $|a_{2n}|$
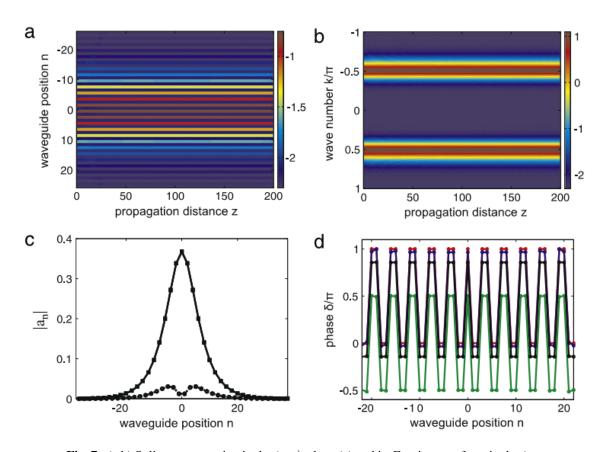
Fig. 7. (a,b) Soliton propagation in the (n, z)-plane (a) and its Fourier transform in the (κ, z)-plane (b) with an even symmetry profile at the input. (c) Absolute values of the field amplitudes for intense ($|a_{2n}|$ with solid line and square markers) and weak ($|a_{2n-1}|$ with dashed–dotted curves and round markers) soliton components at four different values of z =0 (red curves); 50 (blue curves); 140 (green curves); and 200 (black curves). The soliton profile is so well preserved that all these curves just stay on top of each other and one can see only the output black curves. (d) Phase pattern δ/π of soliton profiles at the four above values of z. Colors of curves in (d) have the same meaning as in (c). Parameters: c =1; $\gamma = 1$; $\sigma = -1.2$; and $n_0 = 5$. All contour plots are shown on a logarithmic scale. This figure is reproduced from our original work in Ref. [49].

at even waveguide positions, whereas the weak component with dashed–dotted curves and round markers represents the field profile $|a_{2n-1}|$ at odd waveguide positions. Field profiles in Fig. 7(c) are taken at four values of propagation distance $z = 0$ (red curves); 50 (blue curves); 140 (green curves); and 200 (black curves) –only the black curves are actually visible since the profile is perfectly preserved during propagation with a very high precision. The soliton profile also perfectly preserves its phase pattern across the array (Fig. 7(d)). From Eq. (14), one can easily see that as the waveguide position variable n runs, the phase pattern of the soliton must be periodic as follows: $\delta_n = \cdots(\rho, \rho), (\rho + \pi, \rho + \pi), (\rho, \rho)...$ where ρ also changes with z. This pattern is only broken at the soliton center point where the function *tanh* in Eq. (14) changes its sign. This

phase pattern is shown in Fig. 7(d), where different colors with meanings as in Fig. 7(c) depict pattern at different values of z. The sequence in the phase is important because it allows us to convert Eq. (13) into the nonlinear Dirac equation, as we shall show shortly. Note that the soliton whose propagation is shown in Fig. 7 is the one with even symmetry in Fig. 6(a). Our simulations similarly show that the profile of solitons with odd symmetry in Fig. 6(b) is also well preserved during propagation, and we have checked that this is true even in the presence of quite a strong numerical noise, demonstrating the robustness and the stability of our solutions.

IV.2. Dirac solitons

In this subsection we will report on the simulation of nonlinear relativistic Dirac solitons in BWAs. As shown in Refs. [37, 38], linear CMEs (Eq. (13)) for a beam with phase difference equal to $\pi/2$ can be converted into the linear one-dimensional relativistic Dirac equation (DE). Note that Eq. (13) can be converted into the DE only for beams with special phase patterns; for instance, at normal beam incidence Eq. (13) cannot be converted into the DE. It turns out that with the soliton solution given by Eq. (14), one can also successfully convert Eq. (13) into the nonlinear relativistic Dirac equation (NDE). Thus, one can use BWAs to mimic the relativistic Dirac solitons, and soliton solutions in BWAs given by Eq. (14) can be used to construct directly the Dirac soliton. Although the solution of Eq. (14) does not possess a phase difference equal to $\pi/2$ between adjacent waveguides (see Fig. 7(d)), the fact that it exhibits two wavenumbers $\kappa = \pm\pi/2$ (see Fig. 7(b)) gives us some hope that the NDE can also be obtained in this case. Indeed, this is the case, as shown below. In general, suppose that $[a_{2n}(z), a_{2n-1}(z)]^T = i^{2n}[g(2n, z), q(2n-1, z)]^T$, where the two functions g and q are smooth and their derivatives $\partial_n g$ and $\partial_n q$ exist in the quasicontinuous limit (Eqs. 14) satisfy these requirements). After setting $\Psi_1(n) = (-1)^n a_{2n}$ and $\Psi_2(n) = i(-1)^n a_{2n-1}$, and following the standard approach developed in Refs. [37,38], we can introduce the continuous transverse coordinate $\xi \leftrightarrow n$ and the two-component spinor $\Psi(\xi, z) = (\Psi_1, \Psi_2)^T$ which satisfies the 1D NDE:

$$i\partial_z \Psi = -ic\alpha\partial_\xi \Psi + \sigma\beta\Psi - \gamma G, \tag{15}$$

where the nonlinear term $G \equiv (|\Psi_1|^2\Psi_1, |\Psi_2|^2\Psi_2)^T$, $\beta =$ diag(1,-1) is the Pauli matrix σ_z; and α is the Pauli matrix σ_x with diagonal elements equal to zero, but off-diagonal elements equal to unity. Note that Eq. (15) is identical to the DE obtained in Refs. [37, 38], with the only difference that now we have the nonlinear term G in Eq. (15). Similar soliton solutions have been found for the NDE in Ref. [58], but with a different kind of nonlinearity in the context of quantum field theory. Using the soliton solution given by Eq. (14) and the above relation between a_n and Ψ one can easily obtain the Dirac soliton solution of Eq. (15) as follows:

$$\begin{bmatrix} \Psi_1(\xi, z) \\ \Psi_2(\xi, z) \end{bmatrix} = \begin{bmatrix} \frac{2c}{n_0\sqrt{\sigma\gamma}}\text{sech}\left(\frac{2\xi}{n_0}\right)e^{iz\left(\frac{2c^2}{n_0^2\sigma} - \sigma\right)} \\ i\frac{2c^2}{n_0^2\sigma\sqrt{\sigma\gamma}}\text{sech}\left(\frac{2\xi - 1}{n_0}\right)\tanh\left(\frac{2\xi - 1}{n_0}\right)e^{iz\left(\frac{2c^2}{n_0^2\sigma} - \sigma\right)} \end{bmatrix}. \tag{16}$$

The above solution is obtained for $\sigma¿0$ and $\gamma > 0$. One can use the symmetry properties of Eq. (13) to construct other Dirac soliton solutions of Eq. (15), with different sign combinations between σ and γ (for more details see Ref. [49]). The expressions given by Eq. (16) give the main result of our work in Ref. [49]. The robustness of these Dirac solitons has been numerically demonstrated in Ref. [50]. We have shown in Ref. [50] that even though the initial beam can be

different from the exact Dirac soliton, during propagation in BWAs the beam can gradually evolve toward the exact Dirac soliton. During propagation, it is also possible to form stable structures consisting of many interacting Dirac solitons from inputs made of many quasi-solitons that initially have slightly different peak amplitudes [50]. Many interaction features of these solitons are similar to those of NLSE solitons: two in-phase solitons will attract each other and two out-of-phase solitons will repel each other, they can also exchange energy for intermediate values of phase difference between two solitons. However, the interaction behavior of two in-phase discrete spatial solitons in BWAs is quite different from that of two in-phase NLSE solitons at the later stage after the first collision. Unlike two NLSE in-phase interacting solitons where periodic pattern (including collision) is formed, the collision between two solitons in BWAs happens more and more frequently, and finally just one beam is formed [50].

IV.3. Higher-order Dirac solitons

Soliton solutions to the well-known nonlinear Schrödinger equation governing the pulse propagation in an optical fiber have been thoroughly investigated among various classes of solitons [1, 28, 59]. The shape of the fundamental temporal soliton obtained from the NLSE (further referred to as NLS solitons) is described by the hyperbolic function $u(\tau) = \text{sech}(\tau)$. This shape is absolutely retained during propagation of the fundamental NLS soliton along the optical fiber. In light of this, the DS investigated above in the form of Eq. (14) can also be termed as the fundamental DS, because its profile is also conserved during propagation along the longitudinal axis of BWAs. However, apart from the fundamental soliton solution, the NLSE also has so-called higher-order (HO) soliton solutions with initial shapes being described by $N\text{sech}(\tau)$ where N is an arbitrary integer provided that $N \geq 2$ [1, 60, 61] (further referred to as HONLS solitons). Unlike the fundamental NLS soliton, HONLS solitons have profiles which repeat periodically during propagation. Thus, it is natural to expect that in addition to the fundamental DS, one can also have HODSs in BWAs whose profiles repeat periodically during propagation. The aim of our recent work in Ref. [51] is to investigate the properties and dynamics of these HODSs and to compare them with HONLS solitons.

Supposing that a_n is the analytical fundamental DS solution in the form of Eq. (14), we investigate the propagation of the initial beam $a_n \to ra_n$, where $r = 2$. In analogy to HONLS solitons, one can expect that a beam with this initial profile shows the distinguishing feature of HO solitons, i.e., its profile changes in a periodic manner during propagation. Indeed, this is the case as shown in Fig. 8. The propagation of this beam is illustrated in Fig. 8(a) where one can see that the main body of the beam changes periodically during propagation. At first, the beam is compressed in space, then after the maximum compression it broadens again, and after reaching the maximum broadening it gets compressed. The amplitude $|a_n(z)|$ is periodic in z with the period length L=12.6 for the specific set of parameters used in Fig. 8. In Fig. 8(a) one can also see weak radiations emitted from the body of the beam. This radiation is relativistic Zitterbewegung found in BWAs [38].

Fig. 8(b) shows the two components of the beam profile at odd and even waveguide positions n. The strong component with solid curves and square markers represents the field profile $|a_{2n}|$ at even waveguide positions, whereas the weak component with dashed curves and round markers represents the field profile $|a_{2n+1}|$ at odd waveguide positions. Field profiles in Fig. 8(b) are taken at three values of propagation distance within one period: $z_1 = 119.2$ (blue curves — the

beginning of one period); $z_2 = z_1 + 0.5L = 125.5$ (black curves — the middle of this period); and $z_3 = z_1 + L = 131.8$ (red curves — the end of this period). One can see that the red curves (profiles at the end of one period) completely coincide with the blue curves (profiles at the beginning of this period), as a result, one can hardly see the blue curves because they are hidden behind the red curves. Note that in Fig. 8(b) we intentionally select the greater thickness for the blue curves as compared to other curves such that one can still recognize them behind the thinner red curves. From Figs. 8(a) and (b) one can clearly see that at the beginning and the end of one period most of light energy is localized in the central waveguide with position $n = 0$; then during propagation the beam gradually broadens, as a result the light energy is transferred to other waveguides at two sides of the central waveguide; at the middle of this period represented by black curves in Fig. 8(b) most of light energy now is located at two waveguides with position $n = \pm 2$. Note that the initial input profile most resembles the black curves with the only significant exception that the black curve for even component $|a_{2n}|$ has a dip in the center ($n = 0$), whereas the even component of the initial input curve is monotonically decaying from the center. This feature shows that the established periodic pattern is very robust and can be formed from the initial condition which is not the "exact" oscillatory solution. In Figs. 8(c) and (d) we show the propagation of intense even component $|a_{2n}|$, and weak odd component $|a_{2n+1}|$, respectively, for two periods where the periodic pattern during propagation is also clearly illustrated. In Fig. 8(e) we show the propagation of the central part of the beam in Fig. 8(a), but with much longer propagation distance which exceeds any length of a BWA implementation for all current practical purposes. Our simulations show that after radiating some extra energy to the periphery of the BWA at the beginning of the propagation, the periodic regime of the beam is established over long propagation distances without any loss of energy due to radiation. So, this kind of beams can be called higher-order Dirac solitons (HODSs) in BWAs in analogy to higher-order NLS solitons in optical fibers [1,28,59]. Like the soliton order N for HONLS solitons, the parameter r can also be called the "order" of HODSs. It is worth noting that, like the fundamental DS in the form of Eq. (14), those HODSs also satisfy all necessary conditions to convert Eq. (13) into the nonlinear relativistic 1D Dirac equation (see Ref. [49] for more details).

It is well-known that if the NLSE in optical fibers is presented in the dimensionless canonical form, then the period for HONLS solitons is $\pi/2$ in dimensionless unit where the length scale is the dispersion length $L_D = T_0^2/|\beta_2|$ with T_0 being the pulse duration and β_2 being the group velocity dispersion parameter of the fiber [1]. As mentioned above, in the case of NLS solitons in optical fibers, the true HONLS solitons have the order N which is an arbitrary integer provided that $N \geq 2$. In that case the shape of the solitons absolutely repeats after each period $\pi/2$. When the parameter N is not an integer, some weak radiation is emitted continuously from the body of solitons during propagation, but the shape of the central part of solitons also practically repeats after the period $\pi/2$ which is independent of the specific value of N. For HODSs, when the parameter r (which plays the role of the parameter N for HONLS solitons) varies continuously in a certain range the main part of the solitons also repeats periodically during propagation like in the case with $r = 2$ shown in Fig. 8(a), however, the period L does depend on the specific value of r. This nontrivial feature of HODSs is illustrated in Figs. 9(a) – (c) where we show their propagation with different values of the parameter $r = 1.5$, 1.8, and 2.2, respectively. All other parameters in Fig. 9 are the same as in Fig. 8. It is clear that all features in Fig. 8(a) (where the case with $r = 2$ is presented) are reproduced in Figs. 9(a)–(c) (where scenarios with r not being an integer
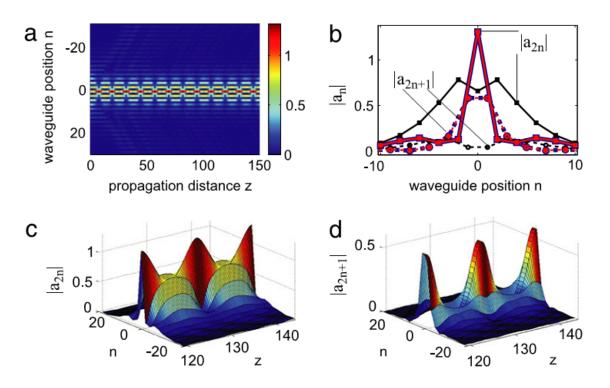
Fig. 8. (a) The propagation of a higher-order Dirac soliton with the parameter $r = 2$. (b) Profiles of the higher-order Dirac soliton at three specific propagation distances within one period: blue curves — the beginning of one period, black curves — the middle of this period, and red curves — the end of this period. (c) The propagation of intense even component $|a_{2n}|$ for two periods. (d) The propagation of weak odd component $|a_{2n+1}|$ for two periods. (e) The same as (a), but with much longer propagation distance. Parameters: $c = 1$; $\gamma = 1$; $\sigma = -1.2$; the beam width parameter $n_0 = 5$; and the order parameter $r = 2$. This figure is reproduced from our original work in Ref. [51].

are presented) with the only exception that the period L in these Figures is different depending on the parameter r. It is important to emphasize that unlike HONLS solitons, in order to obtain HODSs in BWAs the parameter r cannot be too large, otherwise, the periodic change of the HODS amplitudes during propagation will cease to exist from the very beginning as clearly demonstrated in Fig. 9(d) where the propagation of a beam with $r = 3$ (all other parameters are also the same as in Fig. 8) is illustrated. In this case, after a certain propagation distance ($z \simeq 20$ in Fig. 9(d)) most of light energy is just locked in the central waveguide. This feature is due to the discrete nature in BWAs. It is well-known that the discreteness in WAs can create a periodic potential which is known from solid state physics as the Peierls–Nabarro (PN) potential [4]. At high powers like the case shown in Fig. 9(d) the increase of the PN potential results in a strong localization of the beam, mainly in a single waveguide which is effectively decoupled from the rest of the array. For more detailed information on how the period L depends on various parameters such as the order parameter r and the propagation mismatch σ readers can see our original work in Ref. [51].
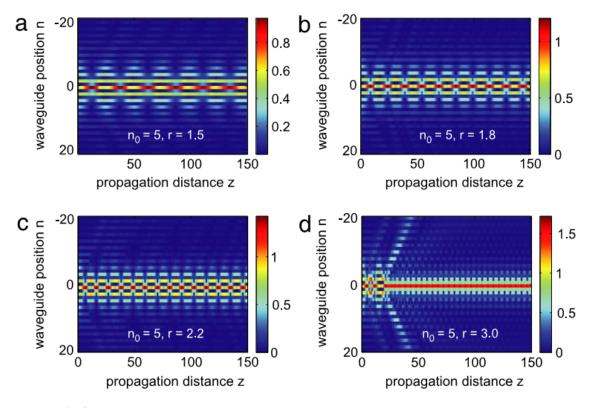
Fig. 9. (a) – (c) The propagation of higher-order Dirac solitons with the order parameter $r = 1.5$, 1.8, and 2.2, respectively. (d) The propagation of a beam with $r = 3.0$. All other parameters are exactly the same as in Fig. 8.

A natural question is what makes HODSs different from HONLS solitons in the sense that the period of the HODSs depends substantially on the order parameter, whereas the period of the HONLS solitons remains constant. One may think that the discreteness of BWAs is the major contributing factor in this matter. However, as clearly shown in [51], this is not the case. So, we conjecture that the binary character (represented by the parameter σ) plays the key role to make the period of HODSs depend on the order parameter r. In addition, when the beam width is large enough, one can convert the CME in WAs (Eq. (13), but with $\sigma = 0$) into the NLSE as shown in [2,62]; however, in BWAs where $\sigma \neq 0$, one can only convert Eq. (13) into the relativistic Dirac equation [49,52], but not into the NLSE. Note also that the NLSE is integrable [1], whereas as far as we know the Dirac equation with Kerr nonlinearity is nonintegrable. This fact is probably the fundamental reason why HODSs are different from HONLS solitons.

In Refs. [49–51] the Dirac solitons in a 1D BWA have been investigated. We have shown in Ref. [52] that Dirac solitons can also exist in square (2D) binary lattices. These 2D Dirac solitons are also quite robust like the 1D counterparts. We have demonstrated in [52] that with the found 2D Dirac solitons, the coupled mode equations governing light dynamics in square binary waveguide lattices can be converted into the nonlinear relativistic 2D Dirac equation with the four-component bispinor.

V. CONCLUSIONS

In this paper we review our works on several new nonlinear effects that we have found in waveguide arrays and in photonic nanowires with sub-wavelength cores. We have shown that for photonic nanowires a new equation should be used to accurately investigate the pulse propagation in the nonlinear regime which takes into account the three following factors at the same time: the vector nature of the electromagnetic modes inside fibers, the strong dispersion of the nonlinearity inside the spectral body of the pulse, and the full variations of the vector mode profiles with frequency. For conventional optical fibers where the core is significantly larger than the wavelength all these three factors are negligible, and thus, one can use the well-known NLSEs to successfully describe the pulse propagation process. However, for photonic nanowires all these three factors are now significant and cannot be ignored anymore. From this new equation we have discovered a new kind of nonlinearity which in some cases can suppress the Raman self-frequency shift of solitons and pulses in nanowires. In WAs we have discovered the diffractive resonant radiation emitted from the discrete solitons. The anomalous recoil effect of this DifRR has also been discovered in this process. In BWAs we have found the optical analogues of both fundamental and higher-order Dirac solitons in quantum relativistic physics in 1D and 2D structures. This paves the way for using binary waveguide arrays and lattices as classical simulators of quantum nonlinear effects arising from the 1D and 2D Dirac equations, something that is thought to be impossible to achieve in conventional (i.e., linear) quantum field theory.

ACKNOWLEDGMENT

REFERENCES

[1] G. P. Agrawal, *Nonlinear Fiber Optics*, 5th ed. (Academic, 2013).
[2] G. P. Agrawal, *Applications of Nonlinear Fiber Optics*, 2nd. (Academic Press, 2008).
[3] D. N. Christodoulides, F. Lederer, and Y. Silberberg, *Nature* **424** (2003) 817.
[4] F. Lederer, G. I. Stegeman, D. N. Christodoulides, G. Assanto, M. Segev, and Y. Silberberg, *Phys. Reports* **463** (2008) 1.
[5] A. Hasegawa and Y. Kodama, *IEEE J. Quantum Electron.* **23** (1987) 510.
[6] J. P. Gordon, *Opt. Lett.* **11** (1986) 662.
[7] A. L. Gaeta, *Opt. Lett.* **27** (2002) 924.
[8] C. M. B. Cordeiro, W. J. Wadsworth, T. A. Birks, and P. St. J. Russell, *Opt. Lett.* **30** (2005) 1980.
[9] P. St. J. Russell, *Science* **299** (2003) 358.
[10] J. M. Dudley, G. Genty, and S. Coen, *Rev. Mod. Phys.* **78** (2006) 1135.
[11] N. Akhmediev and M. Karlsson, *Phys. Rev. A* **51** (1995) 2602.
[12] D. V. Skryabin, F. Luan, J. C. Knight, and P. St. J. Russell, *Science* **301** (2003) 1705.
[13] F. Biancalana, D. V. Skryabin, and A. V. Yulin, *Phys. Rev. E* **70** (2004) 016615.
[14] Tong *et al.*, *Nature* **426** (2003) 816.
[15] F. Benabid, F. Biancalana, P. S. Light, F. Couny, A. Luiten, P. J. Roberts, and A. V. Jiahui Peng, *Opt. Lett.* **33** (2008) 2680.
[16] S. Afshar V. and T. M. Monro, *Opt. Express* **17** (2009) 2298.
[17] M. A. Foster, A. C. Turner, M. Lipson, and A. L. Gaeta, *Opt. Express* **16** (2008) 1300.
[18] M. A. Foster, K. D. Moll, and A. L. Gaeta, *Opt. Express* **12** (2004) 2880.
[19] A. Zheltikov, *J. Opt. Soc. Am. B* **22** (2005) 1100.

[20] Tr. X. Tran and F. Biancalana, *Opt. Express* **17** (2009) 17934.
[21] F. Biancalana, Tr. X. Tran, S. Stark, M. A. Schmidt, and P. St. J. Russell, *Phys. Rev. Lett.* **105** (2010) 093904.
[22] P. V. Mamyshev and S. V. Chernikov, *Opt. Lett.* **15** (1990) 1076.
[23] M. Kolesik and J. V. Moloney, *Phys. Rev. E* **70** (2004) 036604 (2004).
[24] M. Kolesik, E. M. Wright, and J. V. Moloney, *Appl. Phys. B* **79** (2004) 293.
[25] J. Lægsgaard, *Opt. Express* **15** (2007) 16110.
[26] A. L. Jones, *J. Opt. Soc. Am.* **55** (1965) 261.
[27] D. N. Christodoulides and R. I. Joseph, *Opt. Lett.* **13** (1988) 794.
[28] Y. S. Kivshar and G. P. Agrawal, *Optical solitons: From Fibers to Photonic Crystals* (Academic Press, New York, 2003).
[29] T. Pertsch, P. Dannberg, W. Elfiein, A. Brauer, and F. Lederer, *Phys. Rev. Lett.* **83** (1999) 4752.
[30] R. Morandotti, U. Peschel, and J. S. Aitchison, *Phys. Rev. Lett.* **83** (1999) 4756.
[31] M. Ghulinyan, Claudio J. Oton, Zeno Gaburro, and Lorenzo Pavesi, *Phys. Rev. Lett.* **94** (2005) 127401.
[32] H. Trompeter, T. Pertsch, F. Lederer, D. Michaelis, U. Streppel, and A. Bräuer, *Phys. Rev. Lett.* **96** (2006) 023901.
[33] S. Longhi *et al.*, *Phys. Rev. Lett.* **96** (2006) 243901.
[34] Y. Lahini *et al.*, *Phys. Rev. Lett.* **100** (2008) 013906.
[35] S. Longhi, *Phys. Rev. B* **81** (2010) 075102.
[36] F. Dreisow *et al.*, *EPL* **97** (2012) 10008.
[37] S. Longhi, *Opt. Lett.* **35** (2010) 235.
[38] F. Dreisow *et al.*, *Phys. Rev. Lett.* **105** (2010) 143902.
[39] S. Longhi, *Appl. Phys. B* **104** (2011) 453.
[40] J. M. Zeuner *et al.*, *Phys. Rev. Lett.* **109** (2012) 023602.
[41] W. Heisenberg, *Rev. Modern Phys.* **29** (1957) 269.
[42] D. C. Ionescu *et al.*, *Phys. Rev. A* **38** (1988) 616.
[43] A. Zecca, *Internat. J. Theoret. Phys.* **41** (2002) 421.
[44] M. J. Esteban and E. Sere, *Discrete Contin. Dyn. Syst.* **8** (2002) 381.
[45] I. Bialynicki-Birula and J. Mycielski, *Ann. Phys.* **100** (1976) 62.
[46] Tr. X. Tran and F. Biancalana, *Phys. Rev. Lett.* **110** (2013) 113903.
[47] Tr. X. Tran and F. Biancalana, *Opt. Express* **21** (2013) 17539.
[48] Tr. X. Tran and Q. Nguyen-The, *J. Lightwave Technol.* **34** (2016) 4105.
[49] Tr. X. Tran *et al.*, *Ann. Phys.* **340** (2014) 179 – 187.
[50] Tr. X. Tran *et al.*, *J. Opt. Soc. A. B* **31** (2014) 1132-1136.
[51] Tr. X. Tran and D. C. Duong, *Ann. Phys.* **361** (2015) 501-508.
[52] Tr. X. Tran *et al.*, *Phys. Rev. A* **91**, 023814 (2015).
[53] M. D. O'Donnell *et al.*, *J. Am. Ceram. Soc.* **90**, 1448 (2007).
[54] A. V. Husakou and J. Herrmann, *Phys. Rev. Lett.* **87**, 203901 (2001).
[55] V. N. Serkin, T. L. Belyaeva, G. H. Corro, and M. A. Granados, Quantum Electron. **33**, 325 (2003).
[56] J. M. Dudley, G. Genty, and S. Coen, *Rev. Mod. Phys.* **78**, 1135 (2006).
[57] A. A. Sukhorukov and Y. S. Kivshar, *Opt. Lett.* **27**, 2112 (2002).
[58] Y. Nogami, F. M. Toyama, Z. Zhao, *J. Phys. A: Math. Gen.* **28**, 1413 (1995).
[59] V. E. Zakharov and A. B Shabat, *Sov. Phys. — JETP* **34**, 62 (1972).
[60] H. A. Haus and M. N. Islam, *IEEE J. Quantum Electron.* **21**, 1172 (1985).
[61] J. Satsuma and N.Yajima, *Progr. Theoret. Phys. Suppl.* **55**, 284 (1974).
[62] Tr. X. Tran, D. C. Duong, and F. Biancalana, *Phys. Rev. A* **90**, 023857 (2014).